Finite element modeling of jacked piles in clay and loose sand

Ripon Karmaker, Bipul Hawlader & Chen Wang
Memorial University of Newfoundland, St. John's, NL, Canada

ABSTRACT
Pile jacking is one of the alternative pile installation methods to conventional dynamic installations. Jacking does not cause significant vibration or disturbance of the surrounding soil. The present study uses a Coupled Eulerian-Lagrangian (CEL) approach of finite element analysis to simulate the pile jacking process. Quasi-static penetration of a rigid pile in clay and loose sand is simulated. The simulations are performed for an undrained condition for clay and a drained condition for sand. The penetration resistance, penetration-induced radial stress, ground surface heave, and plastic shear strain resulting from pile jacking in clay and sand are compared.

RÉSUMÉ
Le levage de pieux est l'une des méthodes alternatives d'installation des pieux aux installations dynamiques conventionnelles. Le fonçage ne provoque pas de vibrations importantes ni de perturbation du sol environnant. La présente étude utilise une approche d'analyse par éléments finis Coupled Eulerian-Lagrangian (CEL) pour simuler le processus de levage de pieux. La pénétration quasi statique d'un pieu rigide en argile et en sable meuble est simulée. Les simulations sont effectuées pour une condition non drainée pour l'argile et une condition drainée pour le sable. La résistance à la pénétration, la contrainte radiale induite par la pénétration, le soulèvement de la surface du sol et la contrainte de cisaillement du plastique résultant du fonçage de pieux dans l'argile et le sable sont comparés.

1. INTRODUCTION

Dynamic pile driving techniques using hammers or vibrators are commonly used to drive piles. However, the dynamic installation could cause noise, vibration, and even slope failure (e.g., of sensitive clay slopes). The jacking of the pile is an alternative approach to avoid these issues, where a pile is pushed into the soil using a jacking machine up to the jack stroke length, usually at a constant rate.

A large volume of soil displaces when displacement piles (e.g., concrete, closed-ended pipe and plugged open-ended pipe piles) are penetrated into the soil. The displacement of soil could create a number of issues. If the soil has a low hydraulic conductivity (clay), significant excess pore water pressure generates, which cannot dissipate during the period of installation as commonly practiced. This type of penetration could be considered as an undrained loading case. However, for the highly permeable soils (sand), the generated excess pore water pressure would be dissipated; therefore, the drained soil behaviour governs the installations.

The installation of a pile causes a large radial stress increase. At small penetrations, the soil flows outward and upwards, which causes ground surface heave. However, at greater depths, the soil primarily displaces radially; therefore, the cavity expansion theory can be used for modeling the response (Randolph et al. 1979). Using the modified Cam-clay model and assuming the process as an undrained expansion of a cylindrical cavity, Randolph et al. (1979) calculated the radial stress, excess pore water pressure generation, and subsequent consolidation. The concept of cavity expansion has also been used by other researchers (e.g., Basu et al. 2014).

The strain path method (SPM) has also been used to simulate the penetration of piles. Sagaseta and Whittle (2001) modeled the ground movement caused by the installation of piles in clay. They have shown large plastic shear strains around the pile, and their developed SPM could handle such large strains.

The installation of a pile involves a significantly large deformation of soil. The typical finite element (FE) modeling cannot handle such large deformations; therefore, advanced large deformation FE modeling techniques have been used to simulate this process (Qiu et al. 2011; Ko et al. 2016). Note that the penetration of a pile is similar to cone penetration on a small scale. Some studies focused on analytical and numerical modeling of cone penetration in clay and sand (Teh and Houlsby 1991; Wang et al. 2015). Also, field and small-scale laboratory tests were conducted to understand the mechanisms involved in pile installations (Deeks et al. 2005; Yang et al. 2006). The plastic shear strains generated around the pile could reduce the shear strength of the soil. Moreover, the soil displacement could cause ground heave which could be another design issue.

The main objective of the present study to investigate pile installation in clay and loose sand using a large deformation FE modeling technique.

2. PROBLEM STATEMENT

A solid pile of 0.4-m diameter (D) is penetrated into the soil at a constant velocity (v_p) along the z-axis, as shown in Fig. 1. The bottom of the pile is modeled as a half sphere. At any instant, the depth of the pile tip (point T in the inset of Fig. 1) from the ground surface is denoted as w_{tip}. The pile is penetrated to a maximum depth of 10D. The pile penetration in both clay and loose sand is simulated.

Initially, the tip of the pile is placed slightly above the ground surface (w_{tip} = 0.01 mm) to avoid any interaction of the pile with the soil when the soil layer is brought to the in-situ stress condition through a gravity loading step, as discussed later. The groundwater table is considered at the ground surface.

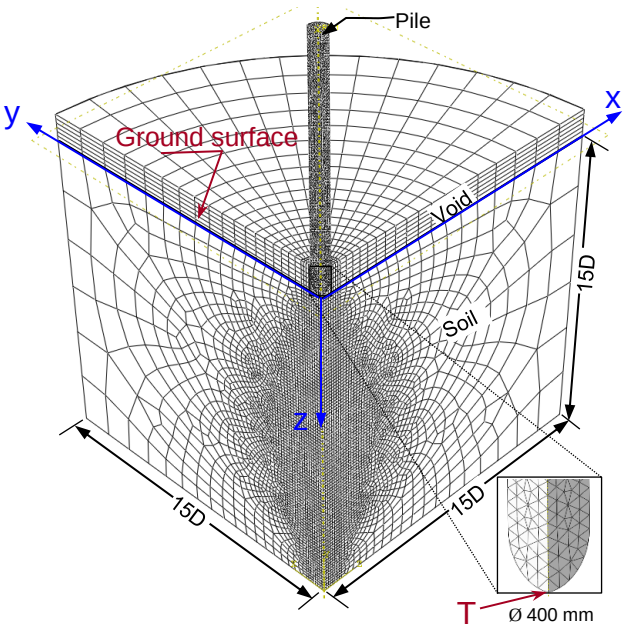

Figure 1: Finite-element mesh

3. FINITE ELEMENT MODELING

The Coupled Eulerian-Lagrangian (CEL) approach available in Abaqus 6.14-2 FE software is used for numerical modeling. One of the main advantages of the CEL is that an extremely large deformation can be simulated without any numerical issues related to mesh distortion, which cannot be performed using a traditional Lagrangian-based FE modeling technique.

Three-dimensional FE analysis is performed by modeling a quarter of the whole domain. The FE mesh used in the analysis is shown in Fig. 1. A dense mesh is used in the zone near the pile where significant soil deformation is expected due to the penetration of the pile. The mesh size is increased with radial distance to reduce the computational time.

The cylindrical boundary is placed at a radial distance of 15*D* from the center of the pile. The height of the soil is 15*D*, which represents that at the maximum penetration depth (w_{tip} = 10*D*), the bottom boundary will be 5*D* far from the tip of the pile. Analyses are also performed with a larger soil domain by placing the boundaries at larger distances and also using finer mesh than that of Fig. 1; however, no significant changes in the result is found. Therefore, the FE mesh shown in Fig. 1 is used.

The soil is modeled as a Eulerian material such that it can flow through the mesh without causing any numerical issue related to mesh distortion (Qui et al. 2011, Karmaker and Hawlader 2018). The pile is modeled as a Lagrangian rigid body. The FE model consists of three parts: soil, pile, and a void. The soil and void for the initial condition are defined by using the Eulerian Volume Fraction (EVF) tool in the software. For a soil element, EVF = 1 means that the element is filled with soil. On the other hand, EVF = 0 represents no soil in the void elements. Note that, during the penetration of the pile, the soil might displace in the void and fill the void element partially (i.e., 0 < EVF < 1.0).

Soil is modeled using the EC3D8R elements, which are 8-node linear multi-material Eulerian brick elements. The pile is first discretized using C3D10M elements, which are 10-node modified quadratic tetrahedrons. The pile is then defined as a rigid body using rigid constraints.

Zero-velocity boundary conditions are used normal to all the vertical faces. In the curved cylindrical outer surface, the soil is allowed to move only in the vertical direction. At the bottom of the domain, zero-velocity boundary conditions are applied in all three directions (i.e. $v_x = v_y = v_z = 0$), meaning that the soil elements next to this boundary are restrained from any movement. No boundary condition is applied at the soil–void interface so that the soil can displace into the void during the penetration of the pile when needed (e.g., ground surface heaving near the pile).

For clay, the analysis is performed for an undrained condition. The soil is modeled as an elastic-perfectly plastic material. Based on the Tresca yield criterion, the yield strength ($\sigma_y = \sqrt{3}s_u$, where s_u is the undrained shear strength of clay) is given as an input. The undrained Young's modulus (E_u) of 500s_u is used. The analysis is performed for s_u = 30 kPa; however, two more analyses are carried out for s_u = 10 and 20 kPa. The undrained Poisson's ratio (ν_u) of 0.49 and submerged unit weight (γ') of 10 kN/m^3 are used. The parameters used in the FE analysis are listed in Table 1.

For sand, the Mohr–Coulomb failure criterion is used to simulate the drained behaviour of loose sand. The angle of internal friction (ϕ') of 32°, which is equal to the critical state friction angle, and the zero dilation angle (ψ) are used (Bolton 1986). The drained Young's modulus (E) of 13.5 MPa and the drained Poisson's ratio of 0.25 are used. A small value of cohesion (c′) is used in the FE analysis in order to avoid numerical issues. The other parameters used in the analysis are listed in Table 1.

Table 1: Geotechnical properties used in FE analysis

	Soil Parameter	Value
Clay	Submerged unit weight, γ' (kN/m^3)	10
	Undrained shear strength, s_u (kPa)	30 (20, 10)
	Undrained Young's modulus E_u	500s_u
	Undrained Poisson's ratio, ν_u	0.49
Sand	Submerged unit weight, γ' (kN/m^3)	7.8
	Drained friction angle, ϕ' (°)	32
	Dilation angle, ψ (°)	0
	Young's modulus E (MPa)	13.5
	Drained Poisson's ratio, ν'	0.25
	Drained cohesion, c' (kPa)	0.1

The pile-soil interface frictional resistance depends on a number of factors, such as surface roughness of the pile, friction angle for the drained condition, and the undrained shear strength for an undrained loading condition. In the present study, the pile–soil interface for clay is modeled as a smooth condition. For sand, an interface friction coefficient μ of 0.3 is taken. Further studies are required to investigate the effects of interface behaviour on pile penetration.

The present FE modeling consists of two loading steps. First, the gravity loading is applied gradually to bring the soil to the in-situ state. At the end of the gravity loading step, the ratio between the horizontal (radial in this case) and vertical stress (K) is $\nu/(1-\nu)$, where ν is the Poisson's ratio. In the second step, the pile is displaced downward at a constant velocity (v_p).

4. RESULTS

In the following sections, the discussion is focused primarily on the force–displacement relation and associated soil failure mechanisms during penetration.

For the undrained penetration in clay, the penetration resistance has two components: (i) the resistance from the shear strength of soil (F_s), and (ii) self-weight, which is similar to buoyancy (F_b). A detailed discussion on interpreting the effects of buoyancy on undrained penetration of an object in soft clay is available in the work of Merifield et al. (2009).

In the present FE analysis, the total resistance (F) for a given pile tip depth (w_{tip}) is obtained from the reaction force at the reference point of the rigid pile. For clay, subtracting F_b from F, the soil resistance is obtained as $F_s = F - F_b$. The soil resistance is then presented as a normalized penetration resistance (N) as $N = F_s/s_u A_p$, where A_p is the cross-sectional area of the pile. The F_b is calculated as $\gamma' A_p w_{tip}$, where $A_p w_{tip}$ represents the volume of the displaced soil.

4.1 Effects of penetration rate

In the field, the pile is jacked at a range of velocities. For example, Yang et al. (2006) jacked the test piles at v_p = 0.017–0.03 m/s. In the present study, the penetration rate effects on soil behaviour, for example, excess pore water pressure generation/dissipation or strain-rate effects on undrained shear strength, are not modeled. However, as the analyses are performed for a quasi-static condition, the penetration velocity should be sufficiently small to minimize the inertia effect.

Figure 2 shows the normalized penetration resistance in clay for three penetration velocities. The lowest penetration velocity (v_p = 0.01 m/s) gives a slightly lower N than that for v_p = 0.1 m/s. Therefore, recognizing a significant increase in computational time with the reduction of v_p, the analyses presented in the following sections are conducted with v_p = 0.1 m/s.

4.2 Comparison with previous numerical and analytical solutions

Figure 3 shows the comparison of the normalized force versus tip depth curves obtained from the present FE analysis and two previous large deformation FE analyses. The calculated resistance shown in Fig. 3 is only due to the tip resistance, because a smooth condition is used for the pipe–soil interface.

Using the implicit remeshing and interpolation technique by small strain (RITSS), Wang et al. (2015) simulated the penetration of a cone in weightless soil (i.e., buoyancy force F_b = 0; therefore, the calculated force is only due to soil resistance). They also simulated cone penetration using CEL. Figure 3 shows that the present CEL results closely match with the CEL results of Wang et al. (2015). The small difference, especially near the ground surface, is potentially due to higher E_u and the shape of the pile tip, a half-sphere in this study, while it is a cone in Wang et al. (2015). Moreover, CEL modeling gives slightly higher N than that of RITSS.

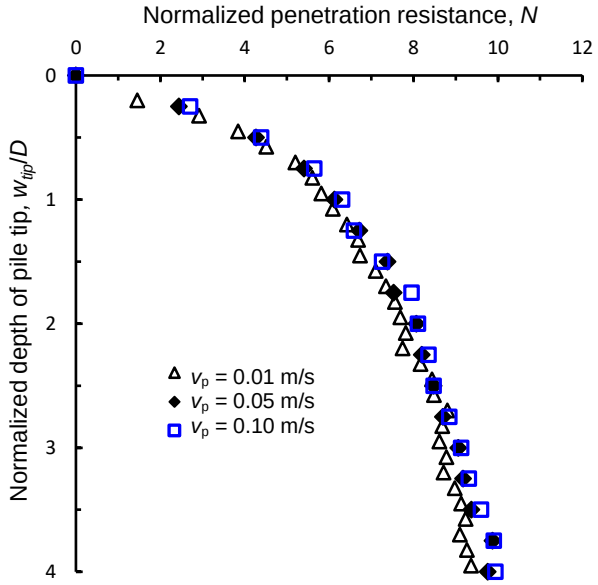

Figure 2: Influence of penetration velocities in CEL analysis

Teh and Houlsby (1991) showed that the normalized cone penetration resistance depends on the rigidity index, I_r (= G/s_u). Some of the smooth cases they analyzed show that N ~ 10–13 for I_r = 100 – 300. In the present study, I_r = 167 is used. Based on theoretical modeling, without simulating a large deformation of the pile, Meyerhof (1951) calculated the normalized ultimate bearing capacity of 9.34 for a deep circular foundation.

While there are some similarities in calculated penetration resistance in different studies, the differences might result from the modeling technique, soil properties and shape of the tip of the penetrating object. These factors influence the soil failure mechanisms during penetration and thereby the penetration resistance.

4.3 Effects of undrained shear strength

In addition to the simulation for s_u = 30 kPa, as discussed above, two more simulations are performed for s_u = 10 kPa and 20 kPa. The Young's modulus is also changed accordingly, maintaining the same rigidity index (= 167). Figure 4(a) shows the penetration resistance (F) with the depth of the pile tip. As expected, F increases with s_u but F is not directly proportional to s_u. However, if the buoyancy component (F_b) is subtracted and normalized (N), the normalized penetration resistance follows an almost single line, as shown in Fig. 4(b). In other words, the penetration resistance only due to undrained shear strength is a

function of N. The maximum N at a deep condition (e.g., $w_{tip} > 7D$) is ~ 10.3.

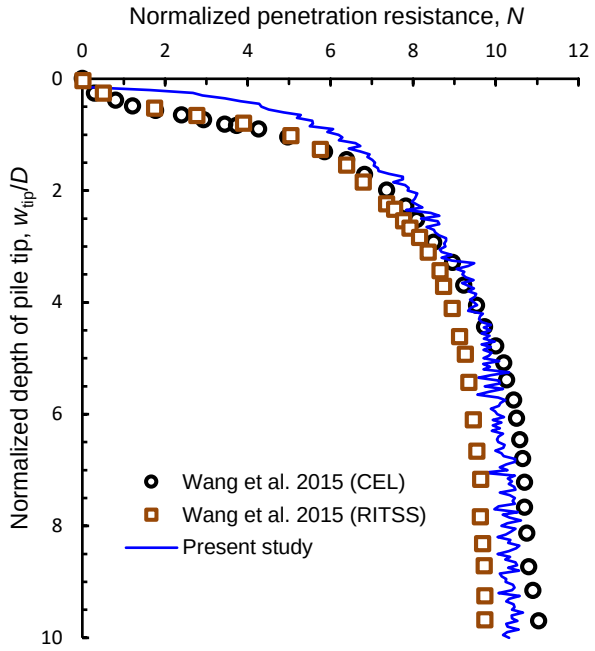

Figure 3: Variation of normalized penetration resistance with a normalized depth of pile tip for clay

4.4 Penetration resistance for sand

Figure 5 shows the penetration resistance (F) in loose sand. In this case, F increases rapidly up to w_{tip} ~ 4.5D and then the rate of increase of F decreases. At $w_{tip} > 4.5D$, the slope of the curve remains constant. A close examination of soil flow around the pile shows that, at $w_{tip} > 4.5$D, the soil failure mechanism is a deep flow mechanism, where the soil flow mainly occurs around the tip of the pile instead of there being any change in flow mechanism. Therefore, the linear increase of F with penetration is due to the increase in vertical stress at the tip and length of the shaft, which increases both tip and shaft resistances.

An analysis is also performed for a smooth pile–soil interface condition. A maximum value of F = 177 kN is found at w_{tip} = 10D, which is 108 kN (= 285 – 177) smaller than the value shown in Fig. 5 at the same tip depth. This difference is the contribution of the shaft resistance.

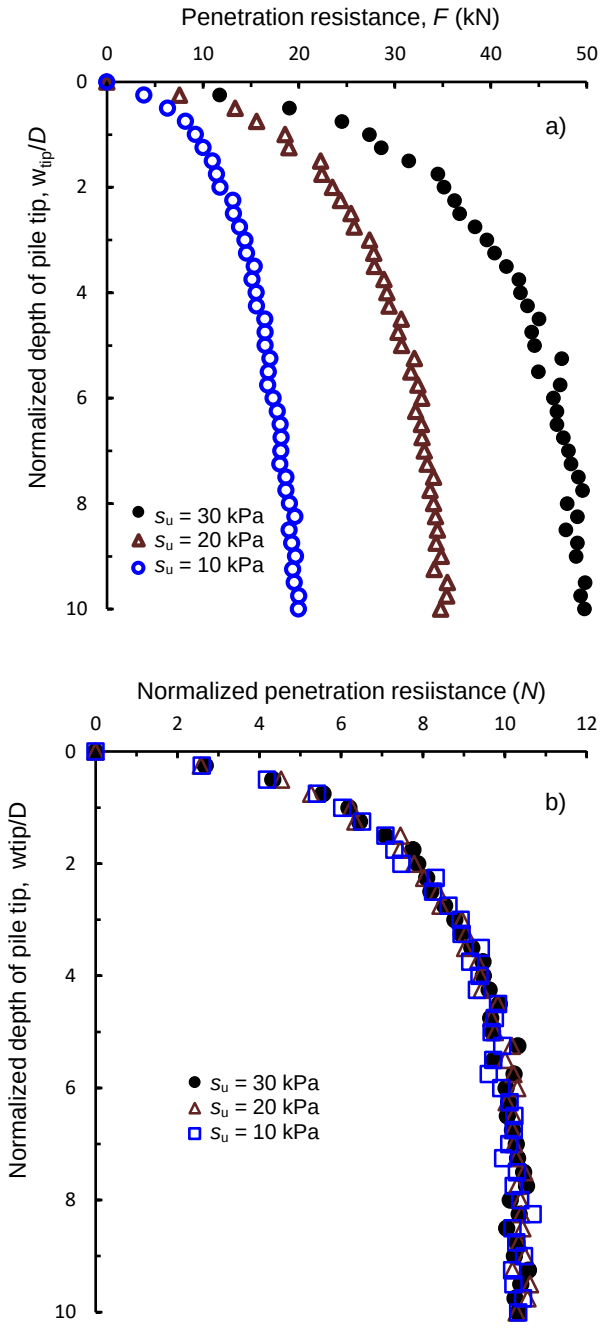

Figure 4: Effects of undrained shear strength of clay on: (a) penetration resistance, (b) normalized penetration resistance

4.5 Radial stresses

The change in radial stress (σ_r) plays a major role in soil failure mechanisms, development of shear strain and pile–soil interface resistance. The variation of radial stress during pile penetration at four depths measured from the initial ground surface (z in Fig. 1) is shown in Fig. 6. The radial distance from the pile surface is plotted in a normalized form ((r-R)/R), where r is the radial distance from the center of the pile and R is the radius of the pile.

Figure 6 shows that the penetration-induced radial stress reaches the maximum when the tip of the pile passes that level. However, the generated radial stress decreases with further penetration. For example, at z = 2.0 m for the pile penetration in clay, the maximum σ_r is 280 kPa (near the pile surface) when the pile tip is at this location (w_{tip} = 2.0 m) (Fig. 6(a)); however, σ_r = 76 kPa when w_{tip} = 3.0 m (Fig. 6(b)). The reduction of σ_r occurs due to stress redistribution during further penetration. Similar behavior has also been observed in sand (Figs. 6(d)–6(f)).

The penetration causes a higher radial stress increase in sand than that in clay, especially at greater depths. Figure 6 also shows that σ_r decreases with radial distance in both sand and clay. However, σ_r decreases faster in sand than in clay. For sand, the penetration-induced radial stress increase is not significant after 5R–10R distance from the pile surface (Figs. 6(d)–6(f)).

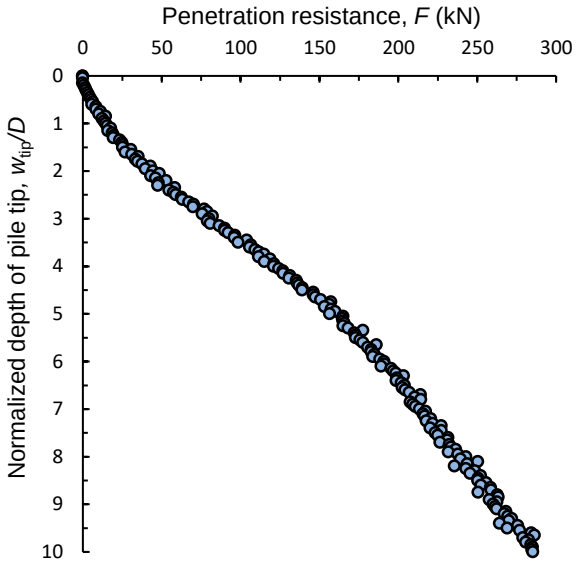

Figure 5: Penetration resistance in loose sand

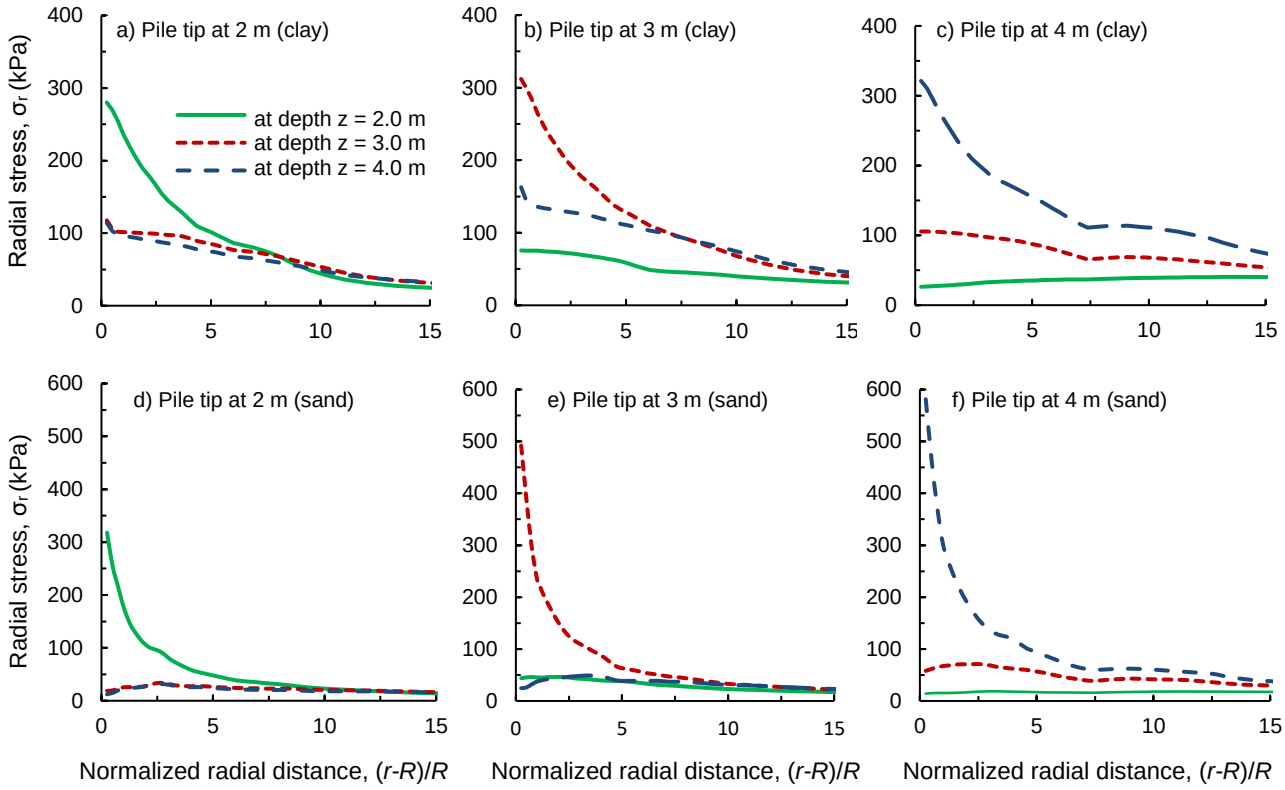

Figure 6: Radial stresses at 2.0, 3.0, 4.0 m depths for different pile tips position: a–c for clay; d–f for sand

4.6 Ground surface heave

Ground heave occurs when a pile is driven into the soil. For example, ~ 400 mm of vertical soil movement was observed at 1.5 m depth when a group of concrete piles was installed in a sensitive marine clay in Quebec (Bozozuk et al. 1978). The heave was negligible further than~ 12 m from the pile group. The occurrence of ground heave has also been reported from many pile installations in clays (e.g., Blanchet et al. 1980; Tomlinson 1957). Ground heave was also observed during the installation of piles in sands (L'Herminier 1953), although the shape and size of the heave in the sand could be different from that observed in clay.

In the present study, the ground surface heave (w_h) is obtained from the deformed ground surface profile of the FE analysis. Figure 7 shows the ground surface heave with the normalized radial distance from the pile ((*r*-*R*)/*R*) for six pile tip depths. For clay, the heave is maximum at ~ 0.5*R* from the pile surface and then decreases rapidly with radial distance and after ~ 3*R* the heave is negligible (Fig. 7a).

For sand, the maximum heave is smaller and occurs at a larger radial distance than that of clay (compare Figs. 7(a) and 7(b)). Moreover, the heave spreads over a larger radial distance in the case of sand.

The magnitude of ground heave increases with penetration depth. For clay, the heave increases until the tip penetration depth of 1.0 m (= 2.5*D*) and no significant change in ground heave occurs during further penetration (Fig. 7(a)).However, the increase of ground heave continues up to 4.0 m penetration of the pile tip in the sand (Fig. 7(b)).

The negative value of w_h close to the pile surface represents a gap between the soil and pile. This gap forms due to soil flow mechanisms during penetration, and the size and shape of the gap depend on soil properties. Note that during the installation of a pile using a hammer, the transverse vibration also helps to form a gap. The separated segment of the pile by the gap does not provide any shaft resistance in the calculated total resistance (*F*), as presented in Fig. 5.

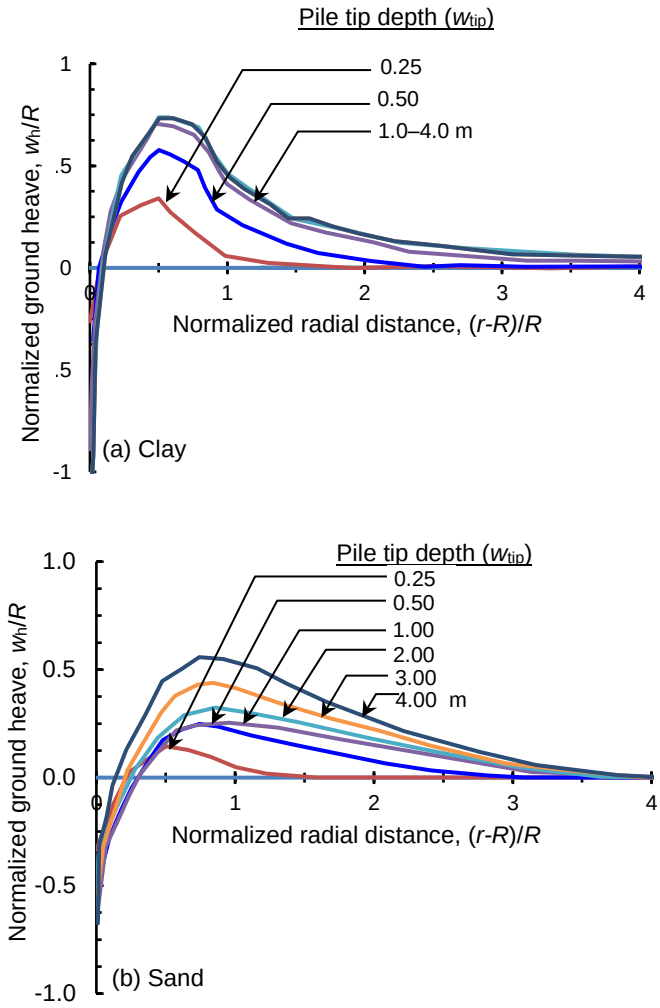

Figure 7: Ground heaves in different soil profiles for various pile tip locations

4.7 Plastic shear strain

Figure 8 shows the equivalent plastic shear strain ϵ_q^p (= PEEQVAVG in Abaqus) with penetration. The plastic shear zone increases with the depth of penetration at shallow depths (e.g., w_{tip} = 1.0 m). However, the width of the plastic shear zone does not increase after a certain depth of penetration. Comparing Figs. 8(a–d) and 8(e–f) for the clay and sand cases, respectively, shows a wider plastic shear zone in the case of clay, especially for deeper penetration, than that of sand.

Based on monotonic expansion of a cylindrical cavity, Randolph and Wroth (1979) suggested that the width of the plastic shear zone (r_p) for undrained penetration in clay can be estimated as $r_p = R\sqrt{G/s_u}$. For the soil parameters listed in Table 1, r_p of 2.58 m (= 12.9*R*) is calculated. The inset of Fig. 8 shows the plastic shear strain at depth *z* = 3.53 m when the pile penetrates to 4.0 m. The plastic shear strain generates up to *r* ~ 12R, although it is negligible after *r* ~ 4*R*.

5. CONCLUSIONS

This paper presents a comparative numerical study of solid pile penetration in clay and loose sand. Considering the hydraulic conductivity of the soils, the clay is modeled in undrained and sand in drained conditions. The pile is penetrated up to ten diameters. The penetration resistance in clay increases with depth and becomes constant. In the case of sand, the penetration resistance continues to increase because of the effective stress increase with depth, which increases the drained shear strength. The normalized penetration resistance obtained from the present FE analysis compares well with previous studies.

A significant increase in radial stress occurs due to the penetration of the pile. The maximum penetration-induced radial stress develops near the pile surface when the pile tip passes that depth. The radial stress decreases with further penetration of the pile. The radial stress decreases faster with radial distance in sand than in clay. The ground surface heave is larger in clay than in sand; however, a wider heave is obtained for sand.

ACKNOWLEDGMENTS

The work presented in this paper has been supported by the Natural Sciences and Engineering Research Council of Canada (NSERC), Equinor, Petroleum Research Newfoundland and Labrador and Mitacs.

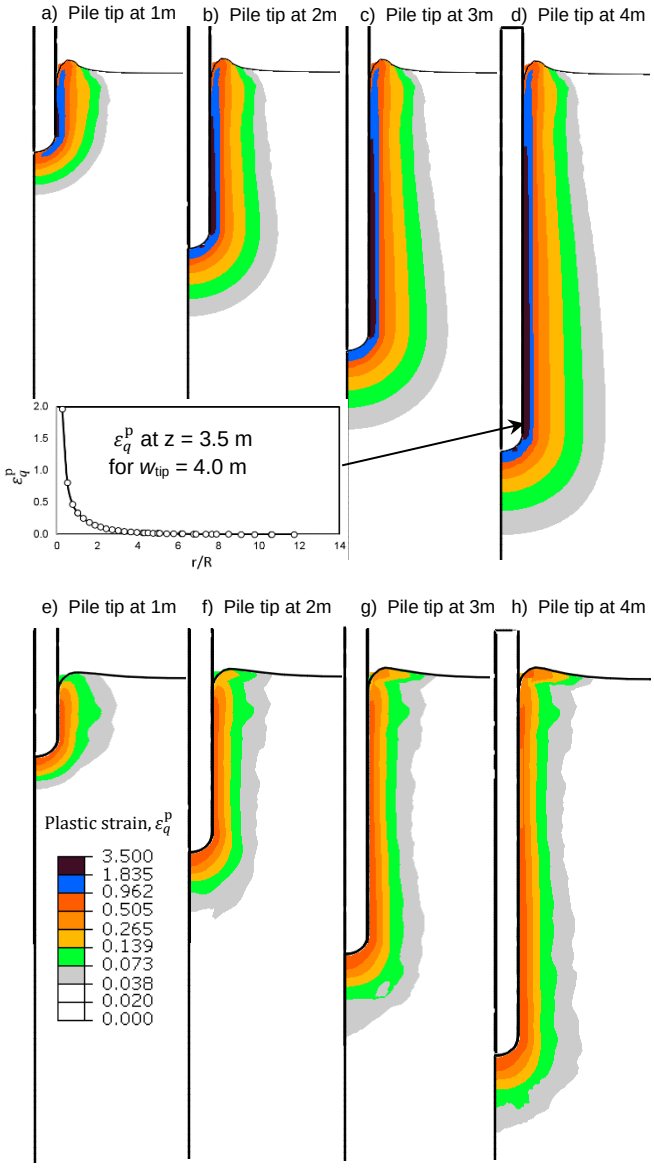

Figure 8: Plastic shear strain with penetration: a–d for clay; e–h for sand

REFERENCES

ABAQUS 6.14 [Computer software]. D. S. Simulia, *Dassault Systémes*.

Basu, P., Pressi, M. and Salgado, R. 2014. Shaft Resistance and Setup Factors for Piles Jacked in Clay, *Journal of Geotechnical and Geoenvironmental Engineering*, ASCE, 140(3): 04013026.

Blanchet, R., Tavenas, F. and Garneau, R. 1980. Behaviour of Friction Piles in Soft Sensitive Clay, *Canadian Geotechnical Journal*, 17(2): 203–224.

Bolton, M. D. 1986. The Strength and Dilatancy of Sands, *Géotechnique*, 36(1): 65-78.

Bozozuk, M., Fellenius, B. H. and Samson, L. 1978. Soil Disturbance from Pile Driving in Sensitive Clay, *Canadian Geotechnical Journal*, 15: 346–361.

Deeks, A. and White, D. J. 2006. Centrifuge Modelling of Jacked Piles, *6th International Conference on Physical Modelling in Geotechnics*, Hong Kong, 6: 821–826.

Karmaker, R. and Hawlader, B. 2018. Modeling of Pile Stabilized Clay Slopes Using a Large Deformation Finite-Element Method, *7th Canadian Geohazards Conference,* paper no-155.

Ko, J., Jeong, S. and Lee, J.K. 2016. Large Deformation FE Analysis of Driven Steel Pipe Piles with Soil Plugging, *Computers and Geotechnics*, 71: 82–97.

L'Herminier, R. 1953. Remarques sur le Poinqonnement Continue des Sables et Graviers, *Annales de l'Institut Technique du Bfitiment et des Travaux Publics*, 63–64: 377–386.

Merifield, R. S., White, D. J. and Randolph, M. F. 2009. Effect of Surface Heave on Response of Partially Embedded Pipelines on Clay, *Journal of Geotechnical and Geoenvironmental Engineering*, ASCE, 135(6): 819–829.

Meyerhof, G. G. 1951. The Ultimate Bearing Capacity of Foundations, *Géotechnique*, 2(4): 301–332.

Qui, G., Henke, S. and Grabe, J. 2011. Application of a Coupled Eulerian-Lagrangian Approach on Geomechanical Problems Involving Large Deformations, *Computers and Geotechnics*, 38: 30–39.

Randolph, M. F., Carter, J. P. and Wroth, C. P. 1979. Driven Piles in Clay–the Effects of Installation and Subsequent Consolidation, *Géotechnique*, 29(4): 361–393.

Randolph, M. F. and Wroth, C. P. 1979. An Analytical Solution for the Consolidation around a Driven pile, *International Journal for Numerical and Analytical Methods in Geomechanics*, 3: 217–229.

Sagaseta, C. and Whittle, A. J. 2001. Prediction of Ground Movement Due to Pile Driving in Clay, *Journal of Geotechnical and Geoenvironmental Engineering*, ASCE, 127(1): 55–66.

Teh, C. I. and Houlsby, G. T. 1991. An Analytical Study of the Cone Penetration Test in Clay, *Géotechnique,* 41(1): 17–34.

Tomlinson, M. J. 1957. The Adhesion of Piles Driven in Clay Soils, *4th International Conference of Soil Mechanics and Foundation Engineering*, London, 2: 66–71.

Wang, D., Bienen, B., Nazem, M., Tian, Y., Zheng, J., Pucker, T. and Randolph, M. F. 2015. Large Deformation Finite Element Analysis in Geotechnical Engineering, *Computers and Geotechnics*, 65: 104–114.

Yang, J., Tham, L. G., Lee, P. K. K., Chan, S. T. and Yu, F. Behaviour of Jacked and Driven Piles in Sandy Soil, *Géotechnique*, 56(4): 245–259.